



# Strain sensing in underwater acoustics with a hybrid $\pi$ -shifted FBG and different interrogation methods

Hanan M. El-Gammal<sup>1</sup> · Nour Eldin Ismail<sup>2</sup> · Mohamed R. M. Rizk<sup>2</sup> · Moustafa H. Aly<sup>3</sup>

Received: 12 November 2021 / Accepted: 7 February 2022 / Published online: 21 March 2022  
© The Author(s) 2022

## Abstract

Although Piezo-Electric Transducers (PZT) hydrophones are widely accepted and technologically mature in the field of Acoustic Emissions (AE) strain sensing underwater, optical fiber-based sensors are gaining more attraction due to their multiplexing capability, small size, high resolution, high sensitivity and immunity to Electromagnetic Interference (EMI). In this paper, we propose a hybrid Fiber Bragg Grating (FBG) system based on combining two apodized FBGs (AFBGs); named Nuttall and  $\text{Cos}^8$ , separated by a  $\pi$ -phase shift to apply it for underwater strain sensing. This combination results in optimum performance in terms of the reflection properties including high peak reflectivity, narrow Full Width at Half Maximum (FWHM), remarkable side lobes suppression, high roll-off rate, good Ripple Factor (RF) and high Detection Accuracy (DA) as well. In addition, an excellent multiplexing capability, high temperature and strain sensitivities and a stable operation over increased temperatures, strain and pressure levels (up to 250 °C, 1000  $\mu$ strain and 100 MPa) are achieved. Moreover, mechanical analysis and comparisons revealed that the Polymer Optical Fiber (POF) recorded the highest sensitivity among other fiber types and their coatings with a value of 1.43 pm/ $\mu$ strain, making it applicable in the strain sensing in underwater acoustics. Furthermore, in this work, a detailed comparative study is performed between several types of interrogators targeting an optimum interrogator for the strain sensing application in underwater acoustics. The obtained results reveal that the linear edge absorption filter detection method achieves better results among the other types. But, unfortunately, when talking about the multiplexing capability, it shows a remarkable failure. Whereas, the Mach-Zehnder Interferometry (MZI) comes in the second place with higher resolution range ( $10^3$ – $10^4$ ) with tunable sensitivity, fast measurement speed, good long-term stability, high multiplexing capability and medium cost. Accordingly, it could be applicable in the application understudy.

**Keywords** Underwater acoustics · Strain sensors · Fiber Bragg grating (FBG) · Hybrid FBG · Optisystem · Optigrating · Polymer optical fiber (POF) · Interrogator · Mach-Zehnder interferometry (MZI)

---

✉ Moustafa H. Aly  
mosaly@aast.edu

## 1 Introduction

The monitoring and detection of AE in the subsea environment is critical for a variety of applications, including geophysical surveys and security (Marques and Webb 2016), Structural Health Monitoring (SHM), medical diagnosis (Violakis et al. 2020), military and field detection (Meng et al. 2021). The majority of current technology relies on PZT hydrophones, which suffer from many drawbacks such as the sensitivity to Electromagnetic Interference (EMI), poor spatial resolution, large physical size, poor performance in several areas, suitable for single point detection only, need for onsite power and impossible for real-time monitoring applications (Bauk and Ilčev 2021). Moreover, they are not suited for usage within a polymer bonded explosive material, because they can produce heat, sparks or short circuit during operation Kumar and Sreerangaraju (2020). On the other hand, FBG based fiber-optic sensors solve those problems and possess enormous advantages over their electronic counterparts (Kumar and Sreerangaraju 2020; Ma et al. 2011), (Moghadas 2011), (Cusano et al. 2018), and (Gangopadhyay 2004).

Examples of the FBG hydrophones are reported previously to inspect the underwater acoustic signals including Equivalent Phase Shift FBG (EPS-FBG) enclosed in a circle metal disk (Huang et al. 2011), cylindrical FBG of different diameters and coated with different materials (Moccia et al. 2012), Photonic Crystal Fiber-FBG (PCF-FBG) (Johny et al. 2017), and FBG side-hole package with polyamide, gold and titanium coating materials (Kumar et al. 2021). But, none of these sensors proved to have high sensitivity combined with stability and large detection range.

In a previous work (El-Gammal et al. 2015), we performed numerical analysis and comparisons between uniform FBG,  $\pi$ FBG and several types of AFBGs including: Gaussian, Barthan, Hamming (Happ-Genzel), Nuttall-Blackman, raised sine (Hanning), Sinc (Lanczos), Tanh and  $\text{Cos}^8$  (raised cosine). The obtained results revealed that the  $\pi$ FBG solved the sensitivity problem of the traditional uniform FBG (Fink 2012). Introducing various apodization functions minimizes the side lobes of the reflection spectrum, but on the extent of reducing the peak reflectivity (Khan and Islam 2012). Accordingly, the idea was to get an optimum FBG-based sensor which consisted of one Nuttall and one  $\text{Cos}^8$  Apodized FBGs (AFBGs) separated by a pi-phase shift.

In this paper, we are going to apply the proposed hybrid FBG in strain sensing in underwater acoustics and completely analyze its reflection performance (in terms of the peak reflectivity, FWHM, side lobes suppression, roll-off rate, ripple factor and detection accuracy). We also will measure its strain sensitivity, detect its strain and pressure ranges, and check its linearity with the increased strain and pressure either isolated or combined with temperature to assure its accuracy of detection. Moreover, the best fiber type and its coating is investigated based on its strain sensitivity. Furthermore, detecting the best interrogator method is detected which has a good resolution, high sensitivity and fast measuring speed.

The remainder of this paper is organized as follows: Sect. 2 is devoted to modeling the strain sensing in FBG. This is followed by FBG model and analysis in Sect. 3. A simple experimental setup of strain monitoring system for underwater acoustics is presented in Sect. 4. The obtained results are displayed and discussed in Sect. 5. In Sect. 6, analysis of the interrogation methods is comparatively explained. Finally, the main conclusions are presented in Sect. 7.

## 2 Modeling of strain sensing in FBG

### 2.1 Strain sensing in FBG

Any strain perturbation that can change the effective refractive index of optical mode propagating along the fiber ( $n_{eff}$ ) and the grating period ( $\Lambda$ ) results in a shift in Bragg wavelength ( $\lambda_B$ ) based on (Hill et al. 1978).

$$\lambda_B = 2n_{eff}\Lambda \quad (1)$$

For accurate strain measurement, the FBG must be isolated from the temperature, which is considered a very ideal case. Once isolated, the grating will respond strictly to strain. Thus, the strain response caused by the sensor's physical elongation can be expressed as (Othonos and Kalli 1999):

$$\frac{\Delta\lambda_B}{\lambda_B} = (1 - \rho_e)\varepsilon_z \quad (2)$$

$$\varepsilon_z = \frac{\Delta\Lambda}{\Lambda} \quad (3)$$

$$\rho_e = \frac{\Delta n}{n} = \frac{n_{eff}^2}{2} [p_{12} - \nu(p_{11} + p_{12})] \quad (4)$$

Thus, Eq. (2) becomes:

$$\Delta\lambda_B = \lambda_B \left( 1 - \frac{n_{eff}^2}{2} [p_{12} - \nu(p_{11} + p_{12})] \right) \frac{\Delta L}{L} \quad (5)$$

where  $\Delta\lambda_B$  is the change in the Bragg wavelength,  $\rho_e$  is the photo-elastic (or strain-optic) constant,  $\varepsilon_z$  is the shear strain in z-direction,  $\Delta\Lambda$  is the change in the grating period,  $\Delta n$  is the change in the amplitude of the induced refractive index,  $n$  is the amplitude of the induced refractive index,  $p_{11}$  and  $p_{12}$  are the strain optic tensor (photo-elastic) coefficients,  $\nu$  is Poisson's ratio,  $L$  is the grating length and  $\Delta L$  is the change in the grating length.

Figure 1 illustrates the modulating of the FBG by the strain variation (compression, zero strain and tension) and the corresponding shift of Bragg wavelength in the reflection spectrum.

In our research work, we will focus on the application of the underwater acoustics measurements. So, we are more concerned with the pressure than the strain. The requirements for a system capable of sensing ultrasonic acoustic waves differ from those for more typical strain and temperature systems. Since the frequency range is much higher (in the range of 100 kHz to several MHz), the pressure range is also higher (in the range of MPa) and the range of the strain is much lower (in the range of  $\mu$ strains) (Betz et al. 2003).

In order to deduce the pressure response caused by the sensor's physical elongation, we will use the relation between the induced strain ( $\varepsilon$ ) and the pressure ( $P$ ) (Fomitchov 2003):

$$P = -\frac{\varepsilon E}{1 - 2\nu} \quad (6)$$

where  $E$  is the Young's modulus of elasticity.

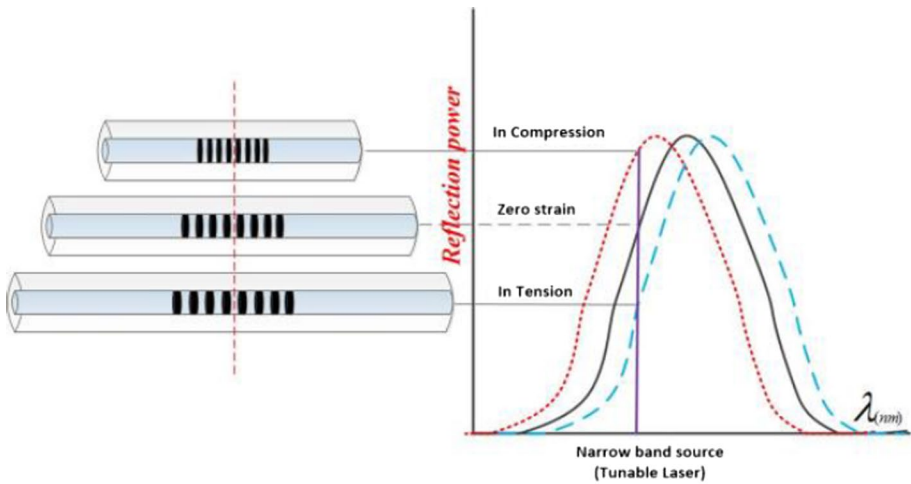


**Fig. 1** Modulation of FBG by the strain variation and the corresponding shift of Bragg wavelength in reflection spectrum (Salih et al. 2016)

In a simple model, the FBG will be assumed to be impinged by a plane ultrasonic pressure wave propagating parallel to the fiber (with inclination angle  $\alpha_{inc}=0^\circ$ ). The differential pressure ( $\Delta P$ ) will be expressed as (Liu and Han 2012):

$$\Delta P(z, t) = \Delta P_o \cos \left( \omega t - \frac{2\pi}{\lambda_s} z \right) \tag{7}$$

where  $\Delta P_o$  is the peak differential pressure,  $\omega$  is the angular frequency,  $t$  is the time and  $\lambda_s$  is the ultrasonic wavelength.

Thus, Eq. (3) becomes:

$$\frac{\Delta \Lambda(z, t)}{\Lambda} = -\Delta P(z, t) \frac{(1 - 2\nu)}{E} \tag{8}$$

and Eq. (4) becomes:

$$\frac{\Delta n(z, t)}{n} = \Delta P(z, t) \frac{n_{eff}^2}{2E} [(1 - 2\nu)(2p_{12} + p_{11})] \tag{9}$$

Finally, one can get the shift in the Bragg wavelength as:

$$\Delta \lambda_B = \lambda_B \left( -\frac{(1 - 2\nu)}{E} - \frac{n_{eff}^2}{2E} [(1 - 2\nu)(2p_{12} + p_{11})] \right) \Delta P(z, t) \tag{10}$$

### 2.2 Quantitative analysis of ultrasonic waves induced strain

Previously, in (Betz et al. 2003) and (Tsuda et al. 2010), mathematical analysis was conducted to assess the strain generated by an ultrasonic vibration. Authors studied the reflection spectrum variation of a launched laser into the FBG resulting from induced strain by

ultrasonic pressure waves. The acoustic wave traveling through water is described as a series of expansions and compressions varying in time, yielding a time-dependent strain field,  $\varepsilon(t)$ . This time-varying strain causes a time-varying wavelength shift,  $\Delta\lambda(t)$ , for the time-varying reflectivity,  $R(t)$ . Thus, the reflectivity is a function of time due to induced ultrasonic-strain is given by:

$$R(t) = R_o + \frac{dR}{d\varepsilon}\varepsilon(t) \quad (11)$$

where  $R_o$  is the reflectivity of the FBG at the lasing wavelength. The laser wavelength was chosen to be in the linear region for accurate detection.

Therefore, from Eq. (11), one can get an expression for the induced ultrasonic-strain in terms of reflectivity as:

$$\varepsilon(t) = [R(t) - R_o] \left( \frac{dR}{d\varepsilon} \right)^{-1} \quad (12)$$

If the output signal is connected to a photodetector, a linear relation will result between the photodetector output voltage,  $V(t)$ , and reflectivity,  $R(t)$ , as follows:

$$V(t) = \frac{V_o}{R_o} R(t) \quad (13)$$

where  $V_o$  is the photodetector output at the lasing wavelength corresponding to  $R_o$ .

By substituting results of Eq. (13) in Eq. (12), one can get:

$$\varepsilon(t) = \left[ \frac{R_o}{V_o} V(t) - R_o \right] \left( \frac{dR}{d\varepsilon} \right)^{-1} = \frac{R_o}{V_o} [V(t) - V_o] \left( \frac{dR}{d\varepsilon} \right)^{-1} \quad (14)$$

By definition, if an ultrasonic pressure is applied on the FBG, the change in strain ( $\Delta\varepsilon$ ) due to pressure becomes:

$$\Delta\varepsilon = \frac{R_o}{V_o} V_{pp} \left( \frac{dR}{d\varepsilon} \right)^{-1} \quad (15)$$

where  $V_{pp}$  is the amplitude of the initial response (peak-to-peak) in the time domain.

Finally, a relation between the strain sensitivity of the Bragg wavelength shift  $\left( \frac{d\lambda}{d\varepsilon} \right)$  and the slope of the FBG reflection spectrum at the lasing wavelength  $\left( \frac{dR}{d\lambda} \right)$  is defined as follows:

$$\frac{dR}{d\varepsilon} = \frac{dR}{d\lambda} \cdot \frac{d\lambda}{d\varepsilon} \quad (16)$$

### 3 FBG model and analysis

#### 3.1 Comparison between different types of fibers and their coatings

Sensor sensitivity, reliability and implementation in different environments are the important parameters to be considered when selecting the correct type of sensor for a specific application. Accordingly, in this section, we are going to compare different types of fibers and their coating materials in order to get the most suitable material

**Table 1** Mechanical properties of different fibers types and their coatings (Marques and Webb 2016; Kumar et al. 2021)

Fiber type	$P_{11}$	$P_{12}$	N	E (GPa)	$\rho$ ( $kg/m^3$ )
Bare fused silica fiber	0.121	0.27	0.17	70	2200
POF	0.300	0.297	0.37	2.95	0.92
Fused silica fiber coated by gold	0.121	0.27	0.44	44	19,280
Fused silica fiber coated by polyamide	0.121	0.27	0.40	3.3	1130
Fused silica fiber coated by titanium	0.121	0.27	0.32	116	$4.512 \times 10^{-6}$
Fused silica fiber coated by acrylate	0.121	0.27	0.37	2.76	1051.1

**Table 2** Strain sensitivity of different fibers types and their coatings

Fiber type	Strain sensitivity ( $pm/\mu strain$ )
Bare fused silica fiber	1.229
POF	1.431
Fused silica fiber coated by gold	1.398
Fused silica fiber coated by polyamide	1.371
Fused silica fiber coated by titanium	1.323
Fused silica fiber coated by acrylate	1.353

for fabricating the FBG strain sensor which can be applicable for sensing underwater acoustic pressure. The different materials of fiber include a bare fused silica fiber and polymer optical fiber (POF), whereas, the different coating materials include gold, polyamide, titanium and acrylate.

The POF has a significantly more flexible nature than silica fiber due to its lower Young's modulus of elasticity. Titanium is exceedingly light, and because of its tensile strength, it can be produced extremely thin. In addition, it possesses the most appealing characteristics of strength, lightness, and flexibility. Polyamide has a low creep and impact strength, is easy to die, and is resistant to a wide range of chemicals. As for gold, it is a ductile and low-impact metal, whereas, acrylates are rubbery, soft and tough class of polymers. They are well-known for their high impact toughness and breakage resistance, as well as their transparency and elasticity.

Table 1 represents the mechanical properties (including the photo-elastic coefficients ( $p_{11}$  and  $p_{12}$ ), Poisson's ratio ( $\nu$ ), Young's modulus of elasticity (E) and Density ( $\rho$ ) for the previously mentioned fibers types and coatings (Marques and Webb 2016; Kumar et al. 2021).

Based on the previously mentioned mechanical parameters, we simulated each fiber type and its coating on the OptiGrating software (ver. 4.2), and used it to calculate the strain sensitivity (in  $pm/\mu strain$ ) for each. The obtained results are summarized in Table 2 and Fig. 2.

From Table 2, one can observe that the POF records the highest sensitivity (1.43  $pm/\mu strain$ ), followed by the gold coated fused silica with the value 1.398  $pm/\mu strain$ . On the other hand, the bare fused silica fiber records the lowest sensitivity (1.229  $pm/\mu strain$ ). The sensitivities of the titanium coated and the acrylate coated fused silica fibers are very close (as shown in Fig. 2).

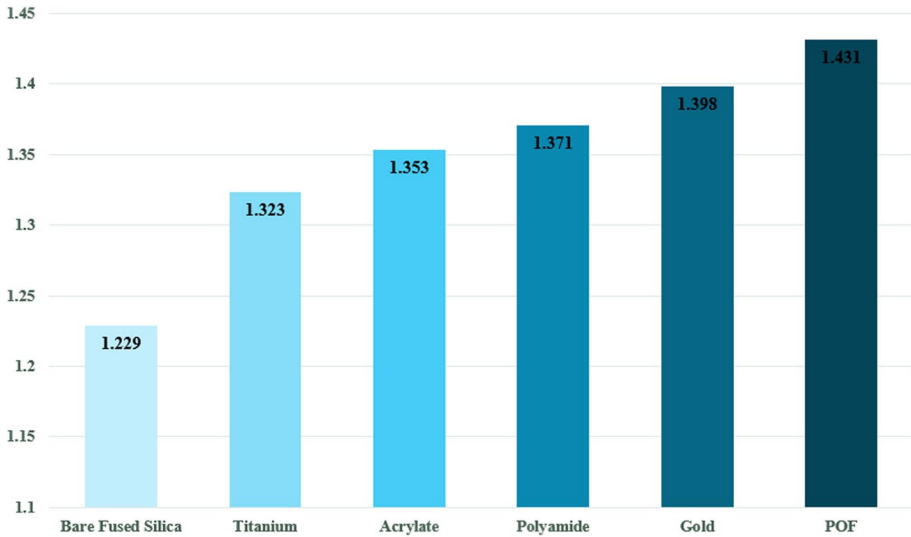


**Fig. 2** Strain sensitivity (pm/μstrain) of different fibers types and their coatings

From these results, one can conclude that the POF is the best type of fibers for the strain sensing. Then comes the fused silica fiber coated by gold in the second place because of its high sensitivity too if the fabrication technology and flexibility of the POF is missing.

### 3.2 The proposed hybrid FBG

Previously, in (El-Gammal et al. 2019), following the mathematical formulations, the OptiGrating software was used to model and analyze the different types of FBGs. The profile type impact on this pattern was evaluated targeting an optimum and a stable sensor. Besides, a comparison was performed between uniform FBG,  $\pi$ FBG and several types of AFBGs including: Barthan, Cos<sup>8</sup> (raised cosine), Gaussian, Hamming (Happ-Genzel), Kaiser, Lorenz, Nuttall-Balckmann, Poisson, raised sine (Hanning), Sinc (Lanczos), Tanh and Welch. The comparison was made at constant grating length ( $L$ ) = 10,000 μm, constant refractive index modulation change ( $\Delta n_{ac}$ ) =  $4 \times 10^{-4}$ , constant room temperature ( $T$ ) = 25 °C and without applying a strain.

The results revealed that although the  $\pi$ FBG has a very high peak reflectivity, ripple factor, good roll-off rate and small number of side lobes, but unfortunately, it shows a remarkable failure when talking about the side lobes analysis and Full Width at Half Maximum (FWHM). Meanwhile, the Nuttall and Cos<sup>8</sup> AFBGs solve this problem on the expense of reflectivity, ripple factor and roll-off rate. Accordingly, the proposed idea was to mix between the three types to form a hybrid FBG to get the optimum performance.

The proposed hybrid FBG results in forming four peak reflectivities in the reflection spectrum with a peak amplitude of 77.63% and achieves a remarkable suppression in the side lobes which is a great progress (with maximum amplitude of -61.173 dB and Side Lobe Suppression Ratio (SLSR) of 95.285%), high ripple factor of 0.97432, narrow FWHM of 1.050 and high Detection Accuracy (DA) of 1476.190 with a fair reflectivity of 77.63% (El-Gammal et al. 2019).

#### 4 FBG strain monitoring system for underwater acoustics

The proposed simple experimental setup of strain monitoring system for underwater acoustics is illustrated in Fig. 3.

Basically, the system in Fig. 3 is composed of an array of FBG sensors inscribed on a fiber optic cable over several kilometers and ended by an Angled Physical Contact (APC) connector to reduce the back-reflections in order to avoid fluctuations in the optical signal due to the formation of Fabry–Perot interferometer between the FBG and the circulator (Takahashi et al. 1999).

The FBG sensors (each with a different Bragg wavelength of  $\lambda_B$ ) are immersed in the water tank in order to monitor the strain resulting from the pressure caused by the acoustic waves. These acoustic waves are generated by the means of PZT ultrasonic probe driven by a function generator and can be visualized on the digital oscilloscope.

Each FBG is enclosed in a metal cylindrical tube in order to improve the sensitivity of the sensor at wide frequency range (2.5–12 kHz) and its multiplexing capability (Huang et al. 2011). In addition, the directionality problem in measuring the AE is solved, where directionality problem results from gluing the grating directly to the inspection surface (Takuma et al. 2014).

The light wave produced by the tunable laser source is fed into the FBG sensor through the optical circulator. Then, the reflected light from the FBG sensor after being subjected to the physical effect (strain only or strain with temperature) passes through the circulator to the 1×2 coupler with a power ratio of 95:5. One of the reflected light beams (of power ratio 95%) is fed into the optical sensing interrogator unit and is being demodulated by the interrogator. The resulting shift in the Bragg wavelength is turned into the form of strain readings which are visualized in the PC. The other reflected light beam (of power ratio 5%) is fed into the photodiode and is then amplified and displayed on the digital oscilloscope.

A simulation of the system is performed by the Optisystem software, version 14.2, and is shown in Fig. 4.

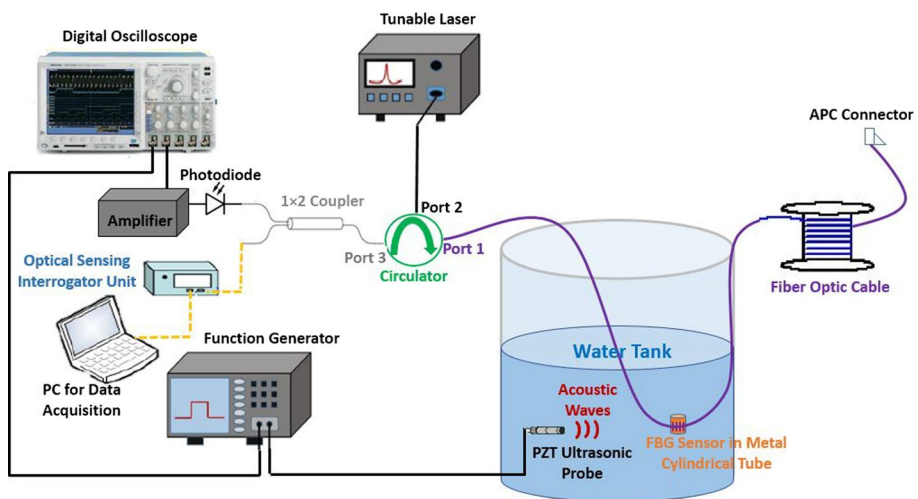
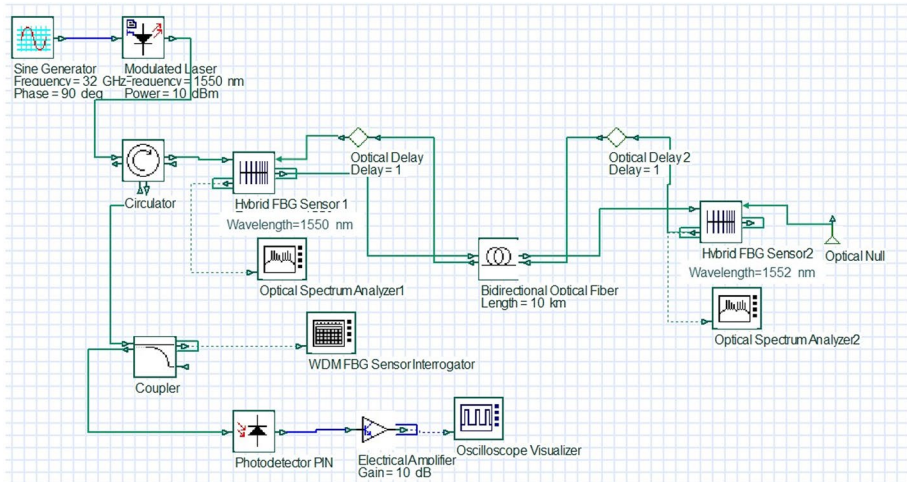


Fig. 3 FBG strain monitoring system for underwater acoustics





**Fig. 4** Simulation of the FBG strain monitoring system for underwater acoustics using Optisystem

The design consists of a modulated laser source of wavelength = 1550 nm and power = 10 dBm, which is being driven by a function generator, generating a sine wave of frequency = 32 GHz and a phase shift =  $90^\circ$ . The laser source illuminates the two hybrid FBG sensors (on which the strain and temperature changes are applied) through the optical circulator. The first FBG has a Bragg wavelength  $\lambda_{B1} = 1550$  nm, while the second has  $\lambda_{B2} = 1552$  nm. The two FBGs are separated by a bi-directional optical fiber of length = 10 km.

An optical delay is added which sends null signals in order to avoid the failure of the simulation when a signal is missing at the input port of any of the hybrid FBG sensors (Razi et al. 2019). The optical null generates a zero-value optical signal to the remaining input port at the end of the system.

The third port of the circulator is connected to a  $1 \times 2$  coupler which divides the power between the WDM FBG sensor interrogator and the PIN photodetector. For displaying the results in the electrical domain, a PIN photodetector is used and is followed by an electronic amplifier. Then, the amplified signal is displayed on the oscilloscope visualizer. Meanwhile, an Optical Spectrum Analyzer (OSA) is added for each FBG sensor to display the optical signal power in the frequency domain as shown in Fig. 5. Finally, the interrogator combines the OSA with analysis tools for locating the maxima or minima of the reflection spectra.

In Fig. 5a, before applying the strain, the power has a peak of about 7 dBm at  $\lambda_B = 1.55 \mu\text{m}$ , while in Fig. 5b, after applying a strain of 1000  $\mu\text{strain}$ , the  $\lambda_B$  is shifted to 1551.53  $\mu\text{m}$  with the same peak power.

## 5 Results and discussions

### 5.1 Effect of the isolated strain ( $\epsilon$ ) on the proposed hybrid FBG

Previously, in (El-Gammal et al. 2019), detailed numerical analysis was performed on the proposed hybrid FBG and the results revealed that it has an optimum performance in terms

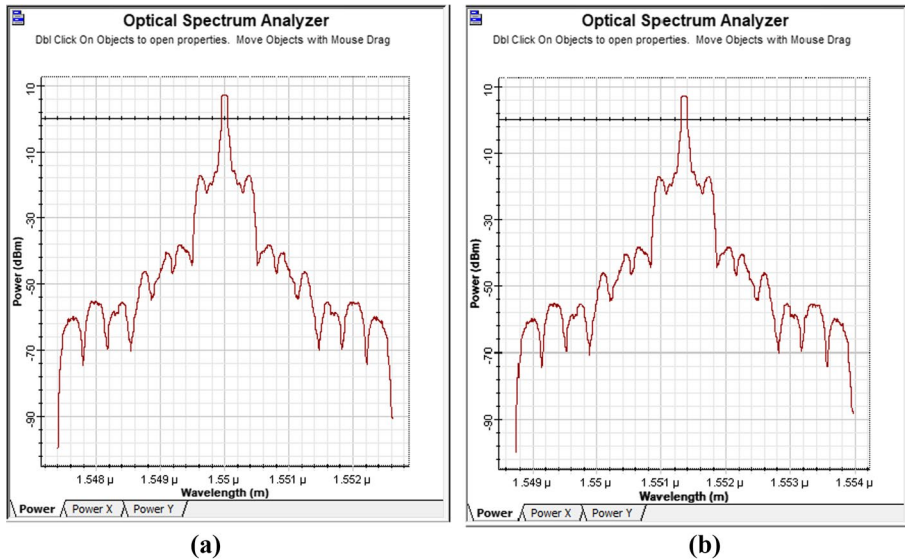


**Fig. 5** The output optical signal of hybrid FBG sensor (1) from the OSA **a** before applying the strain **b** after applying a strain of 1000  $\mu$ strain

of the reflection spectrum properties (including high peak reflectivity, narrow FWHM, remarkable side lobes suppression, high roll-off rate, good ripple factor and high detection accuracy). This FBG was also tested over a wide temperature range (ranging from  $-50$  to  $250$   $^{\circ}\text{C}$ ), showing a stable performance over increased temperature. Based on its performance, the proposed hybrid FBG proved to be applicable in temperature monitoring system for high-voltage OHTLs and bus bars in high-voltage substations for its outstanding performance when compared to the traditional uniform FBG. Now, we will check its stability over the increased strain (or pressure) to investigate if it is still the best solution for the strain sensors array.

Based on previous literature reviews, it was found that the typical hydrophones in underwater acoustics measure pressure ranges up to 100 MPa (Huang et al. 2011). Accordingly, the proposed hybrid FBG will be tested for pressure stability in the range of 0–100 MPa, which is approximately equivalent to a strain range of 0–1000  $\mu$ strain.

New fabricated T100 sensing array by Technica  $^{\circ}$  (Technica 2021) includes FBG sensing elements embedded in single-mode acrylate, polyamide, gold, or other types of coated fiber yielding excellent wavelength to temperature and wavelength to strain linearity with low cost and long lifetime. These sensors can measure a strain up to 10,000  $\mu$ strain and a temperature range from  $-50$  to  $300$   $^{\circ}\text{C}$ . Accordingly, they will match perfectly to our system.

We start with analyzing the FBG strain sensor for underwater acoustics at constant temperature =  $25$   $^{\circ}\text{C}$  (room temperature) in order to isolate the effect of strain from the temperature.

Figure 6 shows the reflection spectrum of the proposed hybrid FBG at constant  $L = 10$  mm,  $\Delta n_{ac} = 4 \times 10^{-4}$  and  $T = 25$   $^{\circ}\text{C}$ , which is being subjected to strain values in the range 0–1000  $\mu$ strain to observe the wavelength shifts. The corresponding center wavelengths at different strain values are illustrated in Table 3.

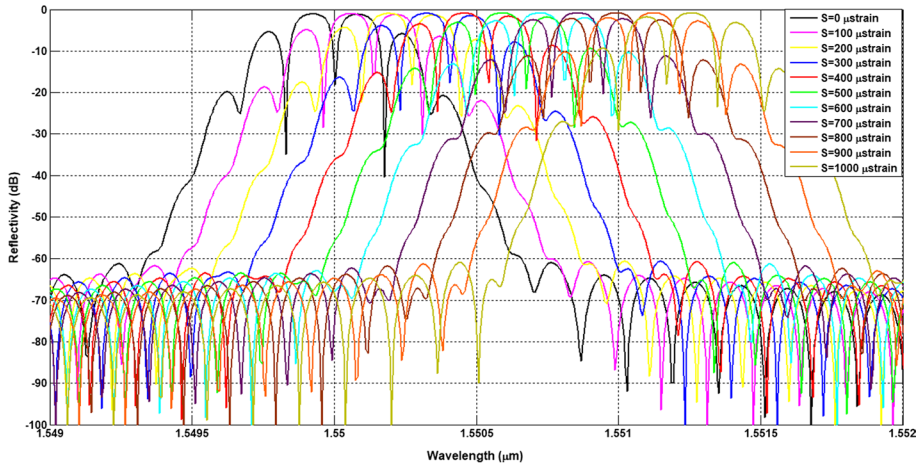


**Fig. 6** Reflectivity for array of the proposed hybrid FBG sensors at different strains at constant  $L = 10$  mm,  $\Delta n_{ac} = 4 \times 10^{-4}$  and  $T = 25$  °C

**Table 3** Center wavelength,  $\lambda_B$ , for the proposed hybrid FBG at constant  $L = 10$  mm,  $\Delta n_{ac} = 4 \times 10^{-4}$  and  $T = 25$  °C, at different values of strain

Strain ( $\mu\text{strain}$ )	Center wavelength (nm)
0	1550.00
100	1550.14
200	1550.272
300	1550.47
400	1550.542
500	1550.677
600	1550.812
700	1550.947
800	1551.079
900	1551.214
1000	1551.349

From Table 3 and Fig. 6, one can conclude that the proposed hybrid FBG has a stable performance over the increased strain (refer to Fig. 7) in case of isolating the effect of temperature.

In addition, the calculated sensitivity of this FBG =  $1.349$  pm/ $\mu\text{strain}$ , which is very close to the sensitivity of the uniform FBG.

The performance of the FBG can be further analyzed based on the Quality Factor (Q) parameter which is defined as the ratio of the sensitivity to FWHM of the Bragg wavelength (Maiti and Singh 2020). The proposed hybrid FBG records a Q of  $0.01285$   $\mu\text{strain}^{-1}$ . Therefore, based on its stable performance, good sensitivity and excellent quality factor can be considered as the best solution for strain sensors array.

Since most of the underwater acoustic measurements' applications are more concerned by the pressure than the strain, accordingly, we are going to study also the

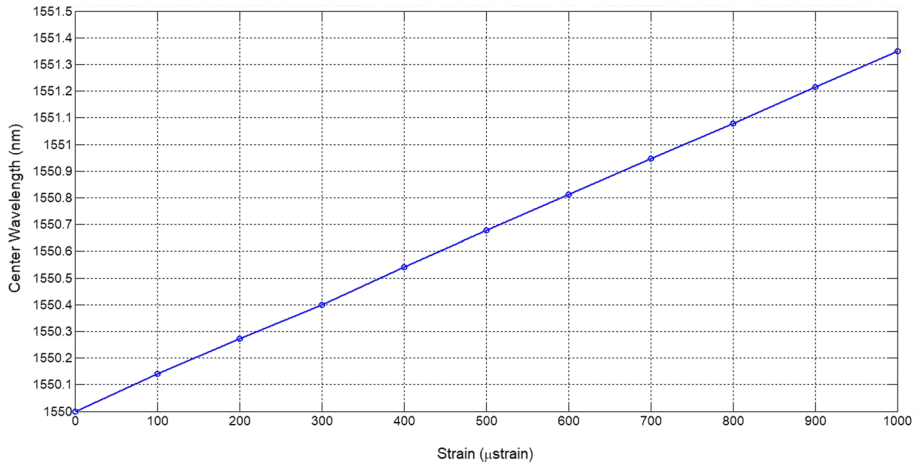


**Fig. 7** Linear relation between center wavelength and strain for the proposed hybrid FBG at constant  $L = 10$  mm,  $\Delta n_{ac} = 4 \times 10^{-4}$  and  $T = 25$  °C

performance of the proposed hybrid FBG over increased pressure in the range 0–100 MPa (traditional hydrophone range) and again in case of isolating the effect of temperature.

The pressure readings are calculated from the strain readings using the relation (refer to Sec. 2.1):

$$P = -\frac{\epsilon E}{1 - 2\nu} \quad (6)$$

The center wavelength at different pressure values is illustrated in Table 4 and Fig. 8 showing a stable performance over the increased pressure.

## 5.2 Physical effect (strain with temperature) on the proposed hybrid FBG

In the previous sections, adequate linearity was obtained by the proposed hybrid FBG when tested under temperature variation only and strain variation only. Now, we are going to prove the system validity in terms of its ability to provide strain and temperature measurement discrimination based on the wavelength shifts induced by both effects simultaneously.

As previously mentioned in (El-Gammal et al. 2019), FBG sensors can be placed in a copper tube in order to avoid the strain effect and study the effect of temperature only. But, in the case of strain measurements, it is hard to isolate the effect of temperature. Accordingly, the wavelength measured is the result of both temperature and strain together, from which, one can subtract the wavelength shift due to temperature only in order to get the accurate wavelength shift due to strain only.

In order to solve this problem, a small modification in the system is made by placing two parallel FBGs: one of them is placed in a copper tube in order to isolate the effect of strain and its wavelength shift due to temperature only; it will be named  $\Delta\lambda_1$ . The other FBG will be free and subjected to the physical effect (temperature and strain together) and

**Table 4** Center wavelength,  $\lambda_B$ , for the proposed hybrid FBG at constant  $L=10$  mm,  $\Delta n_{ac}=4 \times 10^{-4}$  and  $T=25$  °C at different values of pressure

Pressure (MPa)	Center wavelength (nm)
0	1550.00
10.6061	1550.14
21.2121	1550.272
31.8182	1550.47
42.4242	1550.542
53.0303	1550.677
63.6364	1550.812
74.2424	1550.947
84.8485	1551.079
95.4545	1551.214
106.0606	1551.349

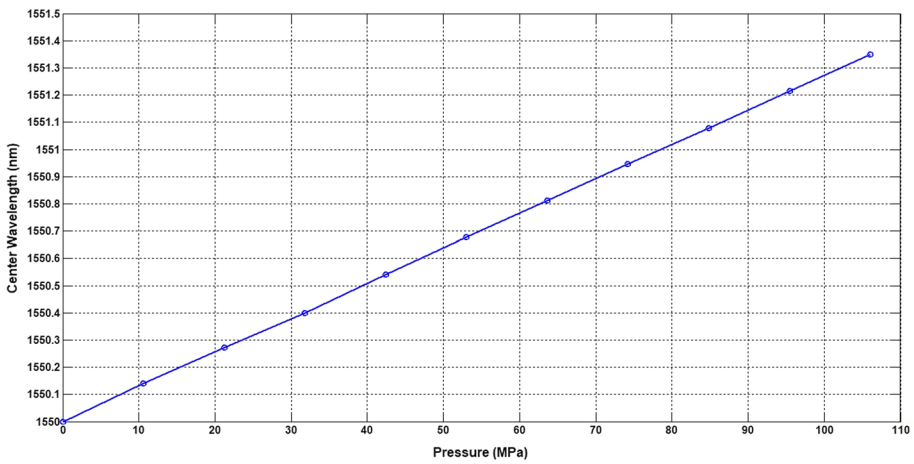


**Fig. 8** Linear relation between center wavelength and pressure for the proposed hybrid FBG at constant  $L=10$  mm,  $\Delta n_{ac}=4 \times 10^{-4}$  and  $T=25$  °C

its wavelength shift due to strain with temperature will be named  $\Delta\lambda_2$ . So, to obtain the wavelength shift due to strain only can simply be calculated using the formula:

$$\Delta\lambda_{strain} = \Delta\lambda_2 - \Delta\lambda_1 \tag{17}$$

Figure 9 shows the linearity of the wavelength shift with the strain applied on the proposed hybrid FBG measured at different temperatures (−50, −25, 0, 25, 50, 100, 200 and 250 °C) with the same slope for all the values, indicating constant sensitivity.

Now, we can conclude that for the strain monitoring system for underwater acoustics application, the proposed hybrid FBG proved to be the optimum solution for this application when compared to the other FBG hydrophones. Those include EPS-FBG enclosed in a circle metal disk (Huang et al. 2011), cylindrical FBG of different diameters and coated with different materials (Moccia et al. 2012), Photonic Crystal

Fiber-FBG (PCF-FBG) (Johny et al. 2017), and FBG side-hole package with polyamide, gold and titanium coating materials (Kumar et al. 2021). This is because none of these sensors has proved to have high sensitivity combined with stability and large detection range.

## 6 Interrogation methods

Interrogation is the most critical operation in the FBG sensing process since it is responsible for decoding the FBG wavelength shifts into a physical effect (temperature or strain for example). The OSA is usually used in the majority of the FBG interrogation systems along with a broadband source (laser or LED) and a circulator. But, unfortunately the OSA has a low resolution, a limited sensitivity, and a slow demodulation speed making it inconvenient in detecting minor and dynamic alterations accurately in the central Bragg wavelengths due to the physical effects. Instead, it can be used for laboratory experiments (Sahota et al. 2020).

Different active and passive interrogation methods have been reported in literature. After several studies, we have chosen to focus on three passive interrogators; power detection method, edge filter method, and Mach-Zehnder Interferometer (MZI) due to their popularity, ease of implementation and small cost, in addition to their high resolution, high sensitivity and fast response time. In our work, we are going to give a brief background on each type, simulate them on the Optisystem software and compare between them in terms of the evaluation parameters targeting a feasible interrogator method, especially in the ultrasonic strain detection which requires a sub-micron-strain resolution, a high bandwidth in the range of kHz, and a fast-scanning time to detect minor wavelength variations (Wu et al. 2018).

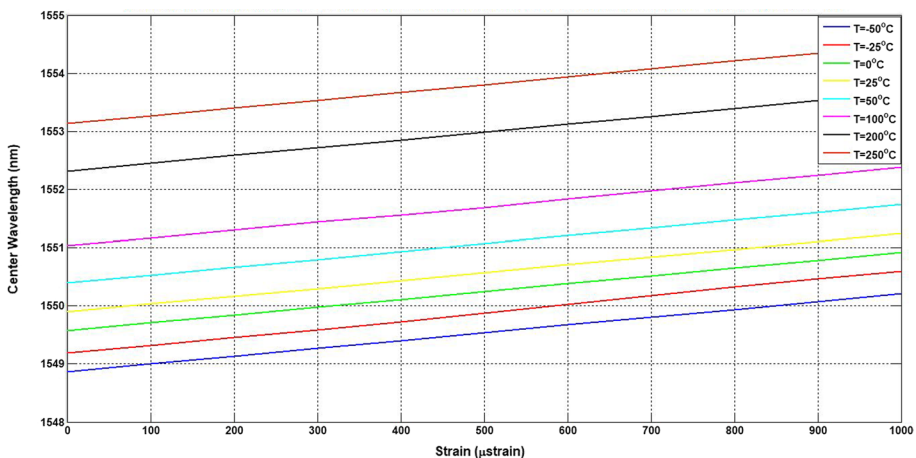


**Fig. 9** Linear relation between center wavelength and strain for the proposed hybrid FBG at constant  $L = 10$  mm and  $\Delta n_{ac} = 4 \times 10^{-4}$ , at different temperatures

## 6.1 Power detection method

This method depends upon the spectral properties of a broadband light source (can be a broadband LED or a narrow bandwidth tunable laser), which is being used to illuminate the FBG and detect the shift in  $\lambda_B$  due to strain variation. Although the multiplexing capability of this method is remarkable, but the sensitivity of this method is low due to the spectral properties of the broadband light source Jinachandran and Rajan (2021).

### 6.1.1 Linear edge power detection method

In the linear edge power detection method, a broadband LED and a FBG are chosen such that the source bandwidth must be greater than the FBG width and  $\lambda_B$  is located at the  $-3$  dB amplitude point of the source (Wild and Hinckley 2010), as shown in Fig. 10a. In this method, the edge of the source is used to detect the strain variation as the  $\lambda_B$  shifts up and down the edge of the source's spectrum resulting in the reflected light intensity variation corresponding to the strain changes (Salih et al. 2016).

The block diagram and simulation of the linear edge power detection method is shown in Fig. 10b. Light signals' paths are colored in red while the electrical signals' paths are colored in green. The broadband light is split into two rays by the means of  $1 \times 2$  coupler, one is being converted to an electrical signal by the means of a photodetector to be displayed on the display, and the other rays act as a sensing element which passes to the optical filter and then to the FBG to detect the strain variation. Then, the reflected ray with the shifted  $\lambda_B$  from the FBG passes back to the optical filter and then to the photodetector through a circulator. The photodetector converts the reflected optical ray into an electrical signal and is being filtered by the means of an electric filter before being displayed. The spectrum shown in Fig. 10a is displayed on the display. Both of optical and electrical filters are driven by a Proportional Integral Derivative (PID) controller in order to minimize the noise resulting from the wavelength difference between the FBG and the source (Cui et al. 2015).

If the light source is considered to have a power spectral density  $PSD_{source}(\lambda)$ , the spectrum of the filter is  $S_{filter}(\lambda)$  and that of the FBG sensor is  $S_{FBG}(\lambda)$  and both have an overlapping area. The response time of the photodetector is  $rt_{photodetector}(\lambda) = \text{Responsivity} \times \text{Resistance}$  of the photodetector. Then, the output voltage from the system displayed on the display is (Lobo et al. 1997; Wu and Okabe 2014):

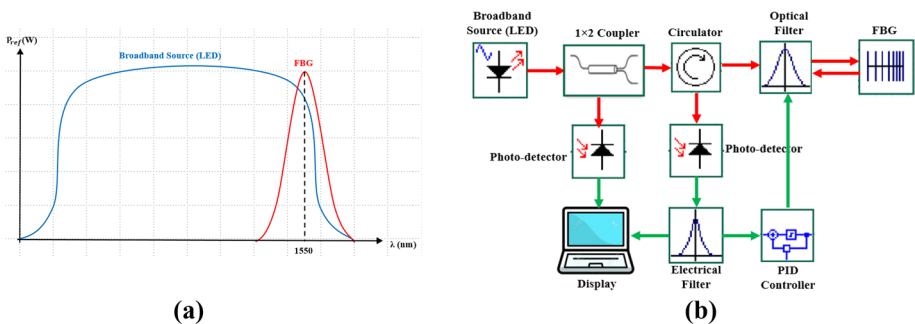


**Fig. 10** Linear edge power detection method: **a** Optical spectrum (Wild and Hinckley 2010), **b** Block diagram

$$V(\Delta\lambda_B) = \int PSD_{source}(\lambda) \cdot S_{filter}(\lambda) \cdot S_{FBG}(\lambda - \Delta\lambda_B) \cdot r_{t_{photodetector}}(\lambda) d\lambda \quad (18)$$

Both  $P_{source}(\lambda)$  and  $r_{t_{photodetector}}(\lambda)$  are considered constants because at a certain wavelength, the power of the light from the source and the photodetector response remains unchanged. When a strain is applied, the spectra of the FBG, the filter will start to separate leading to a decrease in the output power.

### 6.1.2 Narrow bandwidth tunable laser power detection method

On the contrary, in the second power detection method, which is the narrow bandwidth tunable laser method, a very narrow width laser source and a FBG are chosen such that the source bandwidth must be smaller than the FBG FWHM and the source bandwidth is located at the  $-3$  dB amplitude point of the FBG (Salih et al. 2016), as shown in the optical spectrum in Fig. 11a.

The block diagram and simulation of the narrow bandwidth tunable laser power detection method is shown in Fig. 11b. It is similar to that of the linear edge power detection method shown in Fig. 10b, except for the source. Here, the narrow bandwidth tunable laser is being driven by the PID controller. Also, the spectrum shown in Fig. 11a is to be displayed on the display.

## 6.2 Edge filter detection method

This method uses a broadband source and adjusts its wavelength to the linear region of the FBG spectrum. In addition, a spectrally wavelength dependent filter is used to identify any dynamic shifts in the FBG reflection spectrum and turn them into intensity variation. Unlike the power detection method, it has a high sensitivity as the noise level is much lower, but the multiplexing capability of this method is not good enough (Wu et al. 2018).

There is a number of edge filter detection methods under research. But, in our work, we are going to concentrate on only two of them: the matched FBGs which is considered

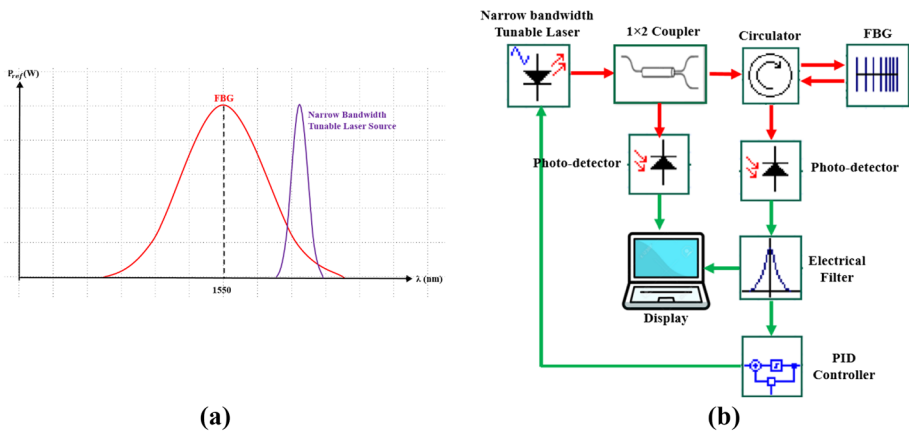


Fig. 11 Narrow bandwidth tunable laser power detection method: a Optical spectrum (Wild and Hinckley 2010, b Block diagram



the simplest detection method and the linear edge absorption filter which is considered the most straight forward detection method (Wild and Hinckley 2010). Others include an interference filter (Cusano et al. 2004), WDM coupler (Ambrosino et al. 2007), an Arrayed-Wave Guide (AWG) (Fujisue et al. 2006), and a Dense WDM (DWDM) filter.

### 6.2.1 Linear edge absorption filter detection method

It is the most straight forward method of the edge filter detection methods. In this method, an external linear edge filter is used, as shown in Fig. 12a. The FBG is chosen such that  $\lambda_B$  is located at the  $-3$  dB amplitude point of absorption transmittance, Fig. 12b, and the light which is not transmitted to the detector is absorbed by the filter (Jinachandran and Rajan 2021).

The block diagram and simulation of linear edge absorption filter detection method shown in Fig. 12a is similar to that of the linear edge power detection method shown in Fig. 10b, except for adding a linear edge filter for the detected signal after being modulated by the strain variation. Again, the spectrum shown in Fig. 12b should be displayed on the display.

If it is considered that the light source has an input power  $P_{source}$ , the grating slope is  $G$  and the responsivity of the photodetector is  $R_{photodetector}$ . Then, the output detected AC signal voltage, which is displayed on the display, is (Bagnoli et al, 2006):

$$V_{AC} = P_{source} \cdot G \cdot R_{photodetector} \cdot \Delta\lambda_B \tag{19}$$

From Eq. (19), it is observed that there is a linear relation between the output detected voltage, the grating slope and the input source power. Accordingly, in order to increase the amplitude of the detected signal, a FBG with a steep slope and a high-power source should be used.

### 6.2.2 Matched FBG

It is the simplest form of the edge filter. In this case, two FBGs are used, one for the sensing (denoted FBG1) and the other is used as a filter (denoted FBG2), which transforms the Bragg wavelength shifts due to strain variation into an intensity variation.

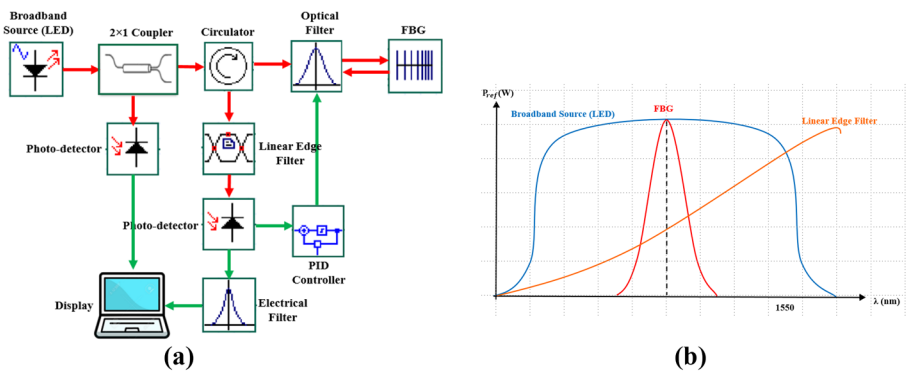


**Fig. 12** Linear edge absorption filter detection method: **a** Block diagram, **b** Optical spectrum (Wild and Hinckley 2010)

If no strain is applied ( $\epsilon=0$ ), the two Bragg wavelengths of the two FBGs will match, and accordingly, no light will be transmitted to the detector, as shown in Fig. 13a. On the other hand, as the strain increases on FBG1, its Bragg wavelength  $\lambda_{B1}$  will shift and the light intensity transmitted by FBG2 will grow gradually.

The main disadvantage of using this method is that it is not easy to identify the strain's nature either it is tensile or compression as the response of both is identical. Besides, the frequency will be doubled. In order to solve these problems,  $\lambda_{B1}$  must be chosen to match the 3 dB amplitude point of the linear edge of FBG2 (Wild and Hinckley 2010). On the other hand, the main advantage of this method is that the temperature variation effect can be eliminated since the temperature changes are the same on both FBG1 and FBG2. So, they both will shift by the same wavelength and cancel each other.

The block diagram and simulation of the matched FBGs detection method is shown in Fig. 13b. It is clear that light from the broadband source could be a LED and is used to illuminate FBG1. Then, the transmitted light from FBG1 is being subjected to strain variation passes through the coupler and reflected to the FBG2 at its  $\lambda_B$ . This reflected light is converted to an electrical signal by the means of a photodetector and is amplified and displayed. Two isolators are placed before and after FBG1 in order to stabilize the sensing signal (Ni et al. 2007).

Consider the incident light intensity is  $I_i(\lambda)$ ,  $R_1(\lambda)$  is the reflectivity of FBG1 and  $R_2(\lambda)$  is the reflectivity of FBG2.  $Att(\lambda)$  is the light power attenuation factor of the light path and the pressure applied on the sensor is  $P=P_A \cos(\omega t)$ , where  $P_A$  is the maximum pressure amplitude. Then, the detected light intensity is given by (Ni et al. 2007):

$$I_d(\lambda) = Att(\lambda) \cdot I_i(\lambda) \cdot [1 - R_1(\lambda - \Delta\lambda_1(p))] \cdot R_2(\lambda + \Delta\lambda_2(p)) \tag{20}$$

### 6.3 Mach-Zehnder interferometer (MZI)

Fiber MZIs are widely utilized for FBG interrogation, especially in strain measurements applications like AE and hydrophones. This is because they possess many advantages over their counterparts such as tunable sensitivity, high resolution, wide bandwidth, fast measuring speed, long-term stability, and multiplexing capability with medium cost.

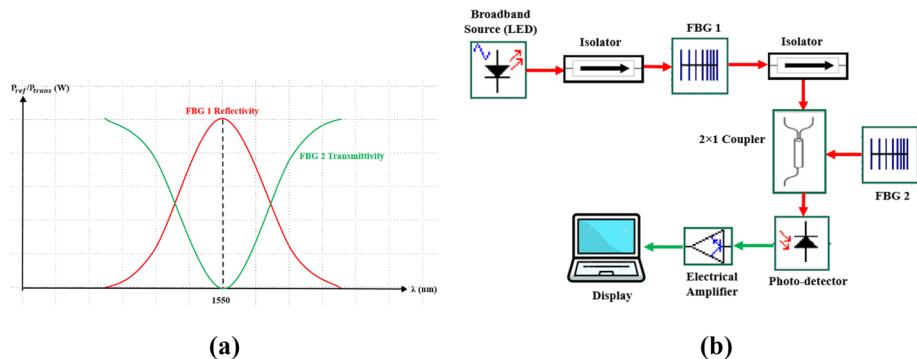


Fig. 13 Matched FBGs detection method: **a** Optical spectrum (Ni et al. 2007), **b** Block diagram

The basic idea of operation of MZI is that it transfers the Bragg wavelength shift of the FBG due to intensity variation into a corresponding phase shift in the electrical domain which can be demodulated using traditional methods (Marques and Webb 2016).

Figure 14 shows an unbalanced MZI detection system. The basic idea of this system is that the MZI converts the Bragg wavelength shift of the emitted laser signal caused strain variation into a phase delay. One arm is the phase modulated and the other is the Optical Path Difference (OPD). The OPD must be adjusted in order to ensure that it is longer than the coherent length of the source and shorter than the coherent wavelength of the reflected light from the FBG in order to avoid visibility reduction and increasing the side lobes level. Some systems represent the OPD as an adjustable air gap.

The modulated laser signal is split and then recombined, thus obtaining a signal proportional to a raised cosine function at the MZI output. The phase depends on the laser wavelength which depends on the strain value applied and also on the OPD. This phase is displayed either on the OSA as an optical signal or on an oscilloscope as an electrical signal.

The phase difference ( $\Delta\phi_{MZI}$ ) is expressed as (Bagnoli et al, 2006):

$$\Delta\phi_{MZI} = \frac{2\pi \cdot OPD}{\lambda_{laser}^2} \Delta\lambda_B \tag{21}$$

where  $\lambda_{laser}$  is the wavelength of the laser signal,  $OPD = n_{co} \cdot L_{unbalance}$ , and  $L_{unbalance}$  is the unbalance length of the two arms.

From Eq. (21), one observes that increasing the unbalance between the arms can increase the sensitivity but to the limit mentioned above. The phase is maintained constant by means of the servo-locking loop at low Fourier frequencies (< 5 kHz) by varying the OPD. The PZT function is to change the OPD by stretching the fiber of one of the arms.

### 6.4 Comparison between different interrogation Methods

Table 5 summarizes the different passive interrogators methods mentioned above based on a market survey performed on the new technologies of FBG interrogators with a number of

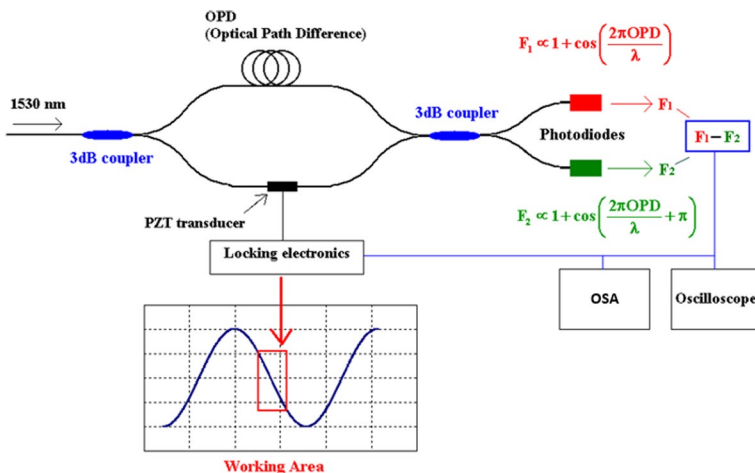


Fig. 14 Mzi detection method (Bagnoli et al. 2006)

key manufacturers including Smart Fibres Limited (Smart Fiber Limited et al. 2021), Technica (Technica 2021), Proximion (Proximion 2021), Advanced Optics Solutions GmbH (Advanced Optics Solutions GmbH 2021), IndiaMART (IndiaMART 2021), and Femto Sensing International (Femto Sensing International 2021).

From Table 5, it is clear that the linear edge absorption filter detection method shows better results among the other types. This is because it has good resolution range ( $10^2$ – $10^3$  fm) with high sensitivity (4.132 dB/nm), fast measurement speed (75 kHz), good long-term stability (up to 35 years) and low cost (~€10,000). But unfortunately, when talking about the multiplexing capability, it shows a remarkable failure (only 3–5 FBGs). Whereas, the MZI can come in the second place with higher resolution range ( $10^3$ – $10^4$  fm) with a tunable sensitivity, fast measurement speed (70 kHz), good long-term stability (up to 25 years), high multiplexing capability (up to 50 FBGs) and medium cost (~€56,600). Accordingly, both of them are applicable in the industrial applications.

## 7 Conclusion

This paper aims to obtain an optimum FBG type as well as a preferable fiber type and its coating for fabricating FBG-based sensors applicable in the advanced application of strain monitoring in underwater acoustics. In addition to an interrogator method that can solve the problem of the traditional interrogator methods using Optical Spectrum Analyzer (OSA). This interrogator should also have a good resolution range with high sensitivity, excellent multiplexing capability, fast measurement speed, good long-term stability and reasonable cost.

The Polymer Optical Fiber (POF) proved to be the preferable fiber type due to its highest sensitivity of value 1.43 pm/ $\mu$ strain, followed by the gold coated fused silica in the second place by the value 1.398.

The proposed hybrid FBG which was introduced in our previous work (El-Gammal et al. 2019), based on the combination of two Apodized FBGs (AFBGs) (Nuttall and Cos<sup>8</sup>) separated by a pi-phase shift, results in forming four peak reflectivities in the reflection spectrum of peak amplitude 77.63% and achieves a remarkable suppression in the side lobes which is a great progress. In addition, the best performance is obtained in terms of side lobes analysis (of 2 with maximum amplitude of –61.173 dB and Side Lobe Suppression Ratio (SLSR) of 95.285%), high Ripple Factor (RF) of 0.97432, narrow Full Width at Half Maximum (FWHM) of 1.050, high Detection Accuracy (DA) of 1476.190, high sensitivity (of 14.557 pm/ °C) and good stability too.

A strain monitoring system for underwater acoustics based on the proposed hybrid FBG is demonstrated. This system proved to be the optimum in strain and pressure sensing due to its excellent reflection properties and strain linearity with the Bragg wavelength shift. Moreover, it has recorded high strain sensitivity of 1.349 pm/ $\mu$ strain and excellent Quality Factor (Q) of 0.01285  $\mu$ strain<sup>-1</sup>. Besides, the system was tested for stability over the range of strains from 0 to 1000  $\mu$ strain and pressure range from 0 to 106.0606 MPa showing excellent results.

The system was tested by the physical effect (strain with temperature) and showed excellent linearity. But a modification is made on the system by placing two parallel FBGs but one of them is temperature isolated and the other subjected to the physical effect.

The linear edge absorption filter detection interrogation method shows better results among the other types. It has a good resolution range ( $10^2$ – $10^3$  fm) with high sensitivity

**Table 5** Comparison between different passive interrogators

Interrogator type	Resolution range (fm)	Sensitivity (dB/nm)	Measurement speed (kHz)	Long-term stability	Multiplexing capability (kHz)	Potential cost (€)
Narrow bandwidth tunable laser power detection	$10^3$ – $10^5$	1.561	100		Good Up to 70 FBGs	€90,000
Linear edge absorption filter detection	$10^2$ – $10^3$	4.132	75	Good (Up to 25 years)	3–5 FBGs	€10,000
Matched FBGs	$10$ – $10^2$	2.932	25	Good (Up to 25 years)	Up to 35 FBGs	€9,000
MZI	$10^3$ – $10^4$	Tunable	70	Good (Up to 25 years)	Up to 50 FBGs	€56,600

(4.132 dB/nm), fast measurement speed (75 kHz), good long-term stability (to 35 years) and low cost (~€10,000). Whereas, the Mach–Zehnder Interferometer (MZI) comes in the second place with higher resolution range ( $10^3$ – $10^4$  fm) with tunable sensitivity, fast measurement speed (70 kHz), good long-term stability (up to 25 years), high multiplexing capability (up to 50 FBGs) and medium cost (~€56,600). Accordingly, both of them are applicable in the industrial applications.

**Funding** Open access funding provided by The Science, Technology & Innovation Funding Authority (STDF) in cooperation with The Egyptian Knowledge Bank (EKB). No organizations funded our research.

## Declarations

**Conflict of interest** The authors declare that there is no conflict of interest regarding the manuscript.

**Open Access** This article is licensed under a Creative Commons Attribution 4.0 International License, which permits use, sharing, adaptation, distribution and reproduction in any medium or format, as long as you give appropriate credit to the original author(s) and the source, provide a link to the Creative Commons licence, and indicate if changes were made. The images or other third party material in this article are included in the article's Creative Commons licence, unless indicated otherwise in a credit line to the material. If material is not included in the article's Creative Commons licence and your intended use is not permitted by statutory regulation or exceeds the permitted use, you will need to obtain permission directly from the copyright holder. To view a copy of this licence, visit <http://creativecommons.org/licenses/by/4.0/>.

## References


- Ambrosino, C., Diodati, G., Laudati, A., Gianvito, A., Concilio, A., Sorrentino, R. and Cusano, A.: Active vibration control using fiber Bragg grating sensors and piezoelectric actuators in co-located configuration. In: Proceedings of SPIE, Third European Workshop on Optical Fibre Sensors, 6619, 661940(1)–661940(4) (2007)
- Advanced Optics Solutions GmbH: <https://www.aos-fiber.com/>. Accessed 12 Nov 2021
- Bagnoli, P.E., Beverini, N., Castorina, E., Falchini, E., Falciai, R., Flaminio, V., Trono, C.: Fiber laser hydrophones as pressure sensors. *Int. J. Mod. Phys. A* **21**, 102–106 (2006)
- Bauk, S. and Ilčev, S. D. In: Proceedings of the 1st International Conference on Maritime Education and Development: ICMED Book (1). Springer, Durban (2021)
- Betz, D.C., Thursby, G., Culshaw, B., Staszewski, W.J.: Acousto-ultrasonic sensing using fiber Bragg gratings. *Smart Mater. Struct.* **12**(1), 122–128 (2003)
- Cui, J., Hu, Y., Feng, K., Li, J., Tan, J.: FBG interrogation method with high resolution and response speed based on a reflective-matched FBG scheme. *Sensors* **2015**(15), 16516–16535 (2015)
- Cusano, A., Cutolo, A., Nasser, J., Giordano, M., Calabro, A.: Dynamic strain measurements by fibre Bragg grating sensor. *Sens. Actuators, A* **110**, 276–281 (2004)
- Cusano, A., Cutolo, A., Albert, J., Araújo, F., Berghmans, F., Bette, S., Campopiano, S., Caucheteur, C., Chen, G., Ferreira, L., Gusarov, A., Ho, S., Ho, T., Iadicicco, A., Kalli, K., Liu, S., López-Amo, M., López-Higuera, J., Mégret, P., Méndez, A., Mezentsev, V., Miller, J., Nasilowski, T., Okabe, Y., Ou, J., Paladino, D., Santos, J., Skaar, J., Staveley, C., Sugden, K., Tam, H., Takeda, N., Webb, D., Wuilpart, M., Zhou, Z.: *Fiber Bragg Grating Sensors: Recent Advancements, Industrial Applications and Market Exploitation*. Bentham e-Books (2018)
- El-Gammal, H.M., Fayed, H.A., AbdEl-Aziz, A., Aly, M.: H: Performance analysis and comparative study of uniform apodized and pi-phase shifted FBGs for array of highperformance temperature sensors. *Optoelectronics Adv Mat Rapid Commun* **9**(9-10), 1251–1259 (2015)
- El-Gammal, H.M., El-Badawy, E.A., Rizk, M.R.M., Aly, M.H.: A new hybrid FBG with a  $\pi$ -shift for temperature sensing in overhead high voltage transmission lines. *Opt. Quant. Electron.* **52**(53), 1–24 (2019)
- Femto Sensing International: <https://femtosing.com/>. Accessed 12 Nov 2021

- Fink T.: Ultrasonic detection using  $\pi$ -phase-shifted fiber Bragg gratings. electrical engineering Theses and Dissertations, Paper 44, University of Lincoln, Nebraska, UK (2012).
- Fomitchov, P.: Response of a fiber Bragg grating ultrasonic sensor. *Opt. Eng.* **42**(4), 956–963 (2003)
- Fujisue, T., Nakamura, K., Ueha, S.: Demodulation of acoustic signals in fiber Bragg grating ultrasonic sensors using arrayed waveguide gratings. *Jpn. J. Appl. Phys.* **45**(5B), 4577–4579 (2006)
- Gangopadhyay, T.K.: Prospects for fiber Bragg gratings and Fabry–Perot interferometers in fibre-optic vibration sensing. *Sens. Actuators, A* **113**(1), 20–38 (2004)
- Hill, K.O., Fujii, Y., Johnson, D.C., Kawasaki, B.S.: Photosensitivity in optical fiber waveguides: application to reflection filter fabrication. *Appl Phys Lett (AIP)* **32**(10), 647–649 (1978)
- Huang, S., Jin, X., Zhang, J., Chen, Y., Wang, Y., Zhou, Z., Ni, J.: An optical fiber hydrophone using equivalent phase shift fiber Bragg grating for underwater acoustic measurement. *Photonic Sens* **1**(3), 289–294 (2011)
- IndiaMART: <https://dir.indiamart.com/>. Accessed 12 Nov 2021
- Jinachandran, S., Rajan, G.: Fibre Bragg grating based acoustic emission measurement system for structural health monitoring applications. *Materials* **14**(4), 897–913 (2021)
- Johny, J., Smith, T., Bhavsar, K. & Prabhu, R.: Design of optical fibre based highly sensitive acoustic sensor for underwater applications. In: *OCEANS 2017*, pp. 1–5, Aberdeen, Scotland (2017)
- Khan, S.S.A., Islam, Md.S.: Determination of the best apodization function and grating length of linearly chirped fiber Bragg grating for dispersion compensation". *J Commun* **7**(11), 840–846 (2012)
- Kumar, H., Sreerangaraju, M.: A comprehensive study on highly sensitive photonics based acoustic sensors for under water applications. *EAI Endors Trans Smart Cities* **4**(12), 1–8 (2020)
- Kumar, H., Sreerangaraju, M.N., Sharan, P.: Characterization of hydroacoustic optical fiber Bragg grating pressure sensor using different materials. *Optics* **2**(20), 100037(1)-100037(6) (2021)
- Liu, M., Han, M.: Analysis of  $\pi$ -phase-shifted fiber Bragg gratings for ultrasonic detection. *IEEE Sens. J.* **12**(7), 2368–2373 (2012)
- Lobo, A.B., Ferreira, L.A., Santos, J.L., Jackson, D.A.: Analysis of the reflective-matched fiber Bragg grating sensing interrogation scheme. *Appl. Opt.* **36**(4), 934–939 (1997)
- Ma, G., Li, C., Quan, J., Jiang, J., Cheng, Y.: A fiber Bragg grating tension and tilt sensor applied to icing monitoring on overhead transmission lines. *IEEE Trans Power Deliv* **26**(4), 2163–2170 (2011)
- Maiti, S., Singh, V.: Performance analysis of apodized fiber Bragg gratings for sensing applications. *SILICON* **2020**, 1–8 (2020)
- Marques, C. A. F. and Webb, D. J.: Fiber Mach–Zehnder interferometer system using polymer optical Bragg grating for underwater applications. In: *Proceedings of 25th International Conference on Plastic Optical Fibres (POF 2016)*, Birmingham, UK 46–52 (2016)
- Meng, Z., Chen, W., Wang, J., Hu, X., Chen, M., Zhang, Y.: Recent progress in fiber-optic hydrophones. *Photonic Sens* **11**, 109–122 (2021)
- Moccia, M., Consales, M., Iadicicco, A., Pisco, M., Cutolo, A., Galdi, V., Cusano, A.: Resonant hydrophones based on coated fiber Bragg gratings. *J. Lightwave Technol.* **30**(15), 2472–2481 (2012)
- Moghadass, A.: Fiber Bragg grating sensor for fault detection in high voltage overhead transmission lines. Ph.D. Thesis, University of Texas at San Antonio, USA (2011).
- Ni, X., Zhao, Y., Yang, J.: Research of a novel fiber Bragg grating underwater acoustic sensor. *Sens Actuators, A* **138**, 76–80 (2007)
- Othonos, A., Kalli, K.: *Fiber Bragg Gratings: Fundamentals and Applications in Telecommunications and Sensing* (1). Artech House Optoelectronics Library, Boston (1999)
- Proximion: <https://www.proximion.com/>. Accessed 12 Nov 2021
- Razi, M.I.M., Beson, M.R.C., Azemi, S.N., Aljunid, S.A.: FBG sensor strain performance analysis using optisystem software tools. *Indones J Electr Eng Comput Sci* **14**(2), 564–572 (2019)
- Sahota, J.K., Gupta, N., Dhawan, D.: Fiber Bragg grating sensors for monitoring of physical parameters a comprehensive review. *Opt Eng* **59**(6), 060901(1)-060901(35) (2020)
- Salih, Y.M., Munajat, Y., Ismail, A.K., Bakhtiar, H.: Response of FBG-bonded plastic plate at different locations of applied stress. *J Teknologi (sci Eng)* **78**(6–11), 77–83 (2016)
- Smart Fiber Limited: <https://www.smartfibres.com/>. Accessed 12 Nov 2021
- Takahashi, N., Tetsumura, K., Takahashi, S.: Underwater acoustic sensor using optical fiber Bragg grating as detecting element. *Jpn. J. Appl. Phys.* **38**(5B), 3233–3236 (1999)
- Takuma, M., Hisada, S., Kenichi, S., Takahashi, Y., Kobayashi, Y., Kadono, A., Murata, A., Iwata, S., Sasaki, T.: Acoustic emission measurement by fiber Bragg grating glued to cylindrical sensor holder. *Adv. Mater. Sci. Eng.* **2014**, 1–12 (2014)
- Technica: T100/FBG Sensing Array. <https://technicasa.com/>. Accessed 9 Sept 2021
- Tsuda, H., Kumakura, K., Ogiwara, S.: Ultrasonic sensitivity of strain-insensitive fiber Bragg grating sensors and evaluation of ultrasound-induced strain. *Sensors* **10**, 11248–11258 (2010)

- Violakis, G., Le-Quang, T., Shevchik, S.A., Wasmer, K.: Sensitivity analysis of acoustic emission detection using fiber Bragg gratings with different optical fiber diameters. *Sensors* **20**(22), 6511–6521 (2020)
- Wild, G. and Hinckley S.: Optical fibre Bragg gratings for acoustic sensors. In: *Proceedings of 20th International Congress on Acoustics (ICA 2010)*, pp. 1–7. Sydney Convention Centre Sydney, New South Wales, Australia (2010)
- Wu, Q., Okabe, Y.: Novel real-time acousto-ultrasonic sensors using two phase-shifted fiber Bragg gratings. *J. Intell. Mater. Syst. Struct.* **25**(5), 640–646 (2014)
- Wu, Q., Okabe, Y., Yu, F.: Ultrasonic structural health monitoring using fiber Bragg grating. *Sensors* **18**(10), 3395–3420 (2018)

**Publisher's Note** Springer Nature remains neutral with regard to jurisdictional claims in published maps and institutional affiliations.

## Authors and Affiliations

Hanan M. El-Gammal<sup>1</sup> · Nour Eldin Ismail<sup>2</sup> · Mohamed R. M. Rizk<sup>2</sup> · Moustafa H. Aly<sup>3</sup> 

Hanan M. El-Gammal  
hanan.elgammal@pua.edu.eg

Nour Eldin Ismail  
nhassan58@live.com

Mohamed R. M. Rizk  
mrm\_rizk@yahoo.com

- <sup>1</sup> Electrical Engineering Department, Faculty of Engineering, Pharos University in Alexandria (P.U.A), Alexandria, Egypt
- <sup>2</sup> Electrical Engineering Department, Faculty of Engineering, Alexandria University, Alexandria, Egypt
- <sup>3</sup> Electronics and Communications Engineering Department, College of Engineering and Technology, Arab Academy for Science, Technology and Maritime Transport, P.O.B. 1029, Abou Kir, Alexandria, Egypt